CARMA INTERFEROMETRIC OBSERVATIONS OF 2MASS J044427+2512: THE FIRST SPATIALLY RESOLVED OBSERVATIONS OF THERMAL EMISSION OF A BROWN DWARF DISK

L. Ricci[1], A. Isella[1], J. M. Carpenter[1], and L. Testi[2]

[1] Department of Astronomy, California Institute of Technology, MC 249-17, Pasadena, CA 91125, USA; lricci@astro.caltech.edu
[2] European Southern Observatory, Karl-Schwarzschild-Strasse 2, D-85748 Garching bei München, Germany

ABSTRACT

We present CARMA 1.3 mm continuum data of the disk surrounding the young brown dwarf 2MASS J044427+2512 in the Taurus molecular cloud. The high angular resolution of the CARMA observations ($0\farcs16$) allows us to spatially resolve for the first time the thermal emission from dust around a brown dwarf. We analyze the interferometric visibilities and constrain the disk outer radius adopting disk models with power-law radial profiles of the dust surface density. In the case of a power-law index $\leqslant 1$, we obtain a disk radius in the range of about 15–30 AU, while larger disks are inferred for steeper radial profiles. By combining this information on the disk spatial extent with the sub-mm spectral index of this source, we find conclusive evidence for mm-sized grains, or larger, in this brown dwarf disk. We discuss the implications of our results on the models of dust evolution in protoplanetary disks and brown dwarf formation.

Key words: brown dwarfs – circumstellar matter – planets and satellites: formation – stars: individual (2MASS J044427+2512) – submillimeter: stars

Online-only material: color figures

1. INTRODUCTION

The investigation of disks around brown dwarfs (BDs) allows us to test the physics of disk evolution and planet formation in physical environments which are very different from those characteristics of disks around young solar-like stars (Luhman et al. 2007b; Apai et al. 2008). In the case of pre-main-sequence (PMS) stars, disks are formed as a consequence of the conservation of angular momentum during the gravitational collapse of the protostellar envelope. Most of the mass forming a newborn star/BD comes from accretion through a circumstellar disk, and characterizing the structure of accretion disks around young BDs has the potential to constrain the mechanisms of their formation (see Luhman 2012).

Disk masses have been measured for a couple of tens of young BDs through far-IR and submillimeter photometry under the assumption of optically thin emission from dust and an interstellar-medium-(ISM)-like dust-to-gas mass ratio (Klein et al. 2003; Scholz et al. 2006; Harvey et al. 2012; Ricci et al. 2012a). However, because of the degeneracy between disk radius and disk surface density and geometry, photometry alone does not provide strong constraints on the radial distribution of mass in the disk. So far, the only direct observational estimate of the radius of a disk around a single young BD has been obtained by Luhman et al. (2007a). They combined *Spitzer* spectroscopy and high-angular resolution imaging with the *Hubble Space Telescope* for the nearly edge-on disk around 2MASS J04381+2611, and inferred a disk radius of about 20–40 AU from the optical images of the disk in scattered light. Also, Ricci et al. (2012a) detected CO molecular gas from the disk surrounding the BD ρ Oph 102 with ALMA at 0.87 mm. They derived a range of possible disk radii: an upper limit of $\approx$30 AU from the non resolved dust emission and a lower limit of $\approx$15 AU from the CO brightness temperature, assuming that this emission is optically thick.

In this Letter, we present the first spatially resolved observations of dust thermal emission from a young BD disk, 2MASS J044427+2512 (hereafter 2M0444). This object

($\approx 0.05\,M_{\odot}$, M7.25-spectral type; Luhman 2004), located in Taurus ($\sim$1 Myr), is known to harbor a disk from its IR excess (Knapp et al. 2004; Guieu et al. 2007; Bouy et al. 2008). We targeted this BD disk, the brightest in the 1.3 mm survey by Scholz et al. (2006), using high-angular resolution ($\approx 0\farcs16$) interferometric observations with the Combined Array for Research in Millimeter-wave Astronomy (CARMA) at a wavelength of about 1.3 mm.

Furthermore, *Spitzer* spectroscopy of this disk provided evidence for μm-sized dust grains, indicating that the very first steps of grain growth have taken place in this system (Bouy et al. 2008). We use our observations and others at sub-mm wavelengths to investigate the presence of larger, mm-sized grains in the outer regions of the 2M0444 disk and test the models of dust evolution in protoplanetary disks.

2. OBSERVATIONS AND DATA REDUCTION

2M0444 was observed with CARMA array configurations A, C, and D, providing baselines lengths between about 11 and 1678 m. Observations in configuration D were obtained on 2011 October 15 and 18. The receivers were tuned at a local oscillator (LO) frequency of 227.5 GHz, correspondent to a wavelength of about 1.318 mm. We set up the CARMA correlator to have a bandwidth of about 6.8 GHz for the continuum, and to observe at the same time the CO ($J = 2 - 1$) molecular line, but no detection was found for this line. We used the same receivers and correlator setup for observations in configuration C on 2012 January 15. Observations in configuration A were carried out on 2011 December 10. The LO was set at a slightly different frequency, i.e., 224.0 GHz, but considering the spectral index of 2M0444 (see below), the flux of the source is expected to vary by <4% at the two different LO frequencies. This is well below the estimated uncertainty in the absolute flux calibration which is about 10% for CARMA.

The frequency-dependent bandpass was calibrated by observing 3C84 and 3C454.3, while the nearby quasar 0510+180 was used to correct for the time-dependent atmospheric and
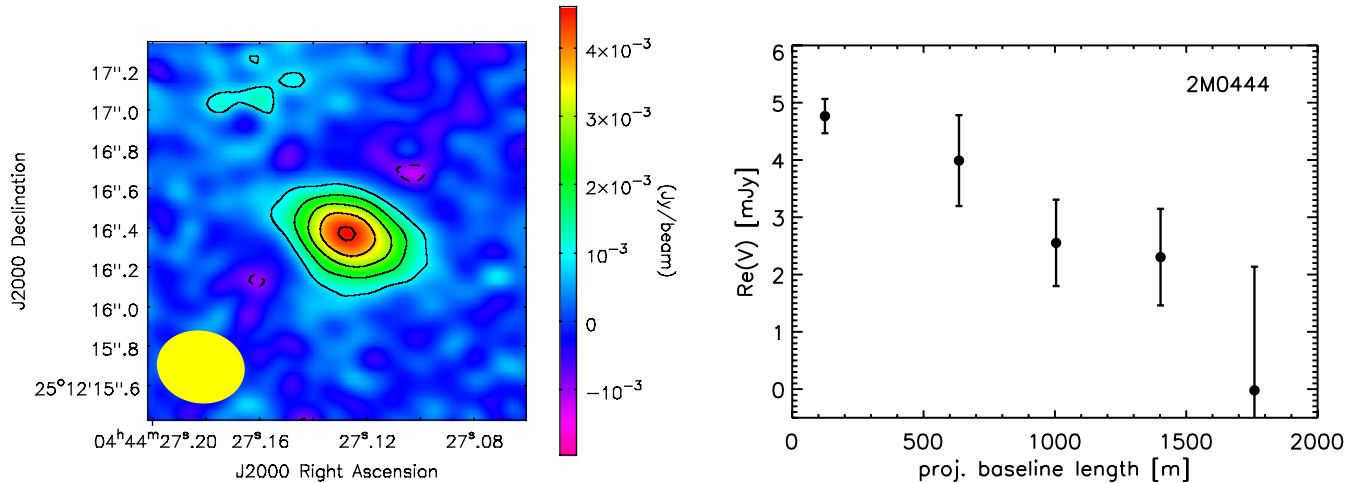
Figure 1. Left: CARMA continuum map at 1.3 mm of the disk surrounding the young brown dwarf 2M0444. This map was obtained by combining all the data taken in configurations A, C, and D of CARMA. Contours are drawn at $-3, 3, 6, 9, 12, 15\sigma$, where $1\sigma = 0.3$ mJy beam^{-1} is the rms noise. The yellow ellipse in the bottom left corner shows the synthesized beam, with FWHM $= 0\farcs36 \times 0\farcs44$, PA $= 80°$, obtained with natural weighting. However, the longest projected baselines of our observations probe angular scales as small as $0\farcs16$. Right: real part of measured visibilities for the 2M0444 disk vs. projected baseline lengths. The points and error bars represent the weighted means of the real parts and their errors, respectively, in the correspondent bins.
(A color version of this figure is available in the online journal.)

instrumental effects. During the observations in configuration A, the quality of these time-dependent corrections were checked by observing the nearby quasar 0431+206, located approximately 5 deg north of 2M0444. This allowed us to quantify to $\lesssim 0\farcs05$ the level of atmospheric seeing during these observations. This is much smaller than the angular resolution of our observations, i.e., $0\farcs16$, showing that the lower visibilities values at longer baseline lengths (Figure 1) cannot be explained by atmospheric decorrelation.

Uranus was used to calibrate the absolute flux scale for observations in configurations D and C, whereas 3C84 was used for data in configuration A, where Uranus is highly resolved. Since 3C84 is known to be a variable source in the millimeter, to evaluate its flux we interpolated between the fluxes measured on December 7 and 15 with the Sub-Millimeter Array (SMA) at about 1.3 mm. We obtained a flux density of about 8.3 Jy for 3C84 on the day of our observations. For all the four epochs of our observations, we shifted the phase center to compensate for the proper motion of 2M0444 ($\mu_\alpha = -1.7$ mas yr^{-1}, $\mu_\delta = -26.5$ mas yr^{-1}, Roeser et al. 2010).

The MIRIAD software package was used for visibilities calibration and imaging. The left panel of Figure 1 shows the 2M0444 map after combining all the data from different array configurations. The integrated flux from the disk is about 5.2 ± 0.3 mJy, where the uncertainty reflects the rms noise on the map.

3. ANALYSIS OF THE OBSERVED INTERFEROMETRIC VISIBILITIES

The right panel of Figure 1 shows the real parts of the measured visibilities versus the projected baseline lengths of our CARMA observations. The decrease at longer baseline lengths indicates that the dust continuum emission of the disk is spatially resolved. This sets a lower limit to the angular extent of the disk, namely the angular resolution of the observations. At the Taurus distance of 140 pc, this corresponds to about 22 AU in diameter or 11 AU in radius.

More precise information on the radial distribution of dust particles can be obtained by analyzing the measured visibilities.

We use the same method adopted by Isella et al. (2009) to fit interferometric visibilities of protoplanetary disks. They used a Markov Chain Monte Carlo (MCMC) to run large collections of disk models, calculated for each disk model the predicted visibilities at the (u, v)-points sampled by their observations, and then derived estimates for the parameters describing the radial distribution of dust in the disk.

To analyze the interferometric visibilities of the 2M0444 BD disk, we used two-layer (surface+midplane) models of flared disks heated by the radiation of the central BD (Chiang & Goldreich 1997; Dullemond et al. 2001). For the (sub-)stellar properties of 2M0444, we adopted an effective temperature $T_{\rm eff} \approx 2838$ K, a luminosity $L_{\rm BD} \approx 0.028\,L_\odot$ as constrained by Luhman (2004), and a distance of 140 pc. By considering the Baraffe et al. (2003) evolutionary models of BDs and an age of 1 Myr, we derived a mass $M_{\rm BD} \approx 50\,M_{\rm Jup}$. This is within 10% from the value of $45\,M_{\rm Jup}$ inferred by Bouy et al. (2008). We calculated the dust opacities κ_ν by considering porous spherical grains made of astronomical silicates, carbonaceous materials, and water ice (optical constants from Weingartner & Draine 2001; Zubko et al. 1996; Warren 1984, respectively), and used a simplified version of the abundances suggested by Pollack et al. (1994) following Ricci et al. (2010a, 2010b). For the grain size distribution, we adopted a power-law $n(a) \propto a^{-q}$ with $q = 3.0$ and truncated between a minimum size of 0.1 μm and a maximum size which sets the value of β ($\kappa_\nu \propto \nu^\beta$, e.g., Ricci et al. 2010b).

We parameterized the surface density of dust in the disk as a truncated power-law in radius $\Sigma(R) = \Sigma_{10\,{\rm AU}}(R/10\,{\rm AU})^{-p}$ from an inner radius $R_{\rm in}$ to an outer radius $R_{\rm out}$. For the disk inner radius we took $R_{\rm in} = 0.05$ AU, which is about the sublimation radius given by the BD properties, but all the parameters considered in our analysis do not significantly depend on the exact value of this parameter. Disk inclination i (angle between disk rotation axis and line of sight) and position angle (P.A., angle between north direction and disk major axis) have been left free to vary in the fitting process. However, disk inclination and position angle were not well constrained by our analysis.

For our analysis we first fixed the value of the power-law index p of the radial profile of the dust surface density. We adopted
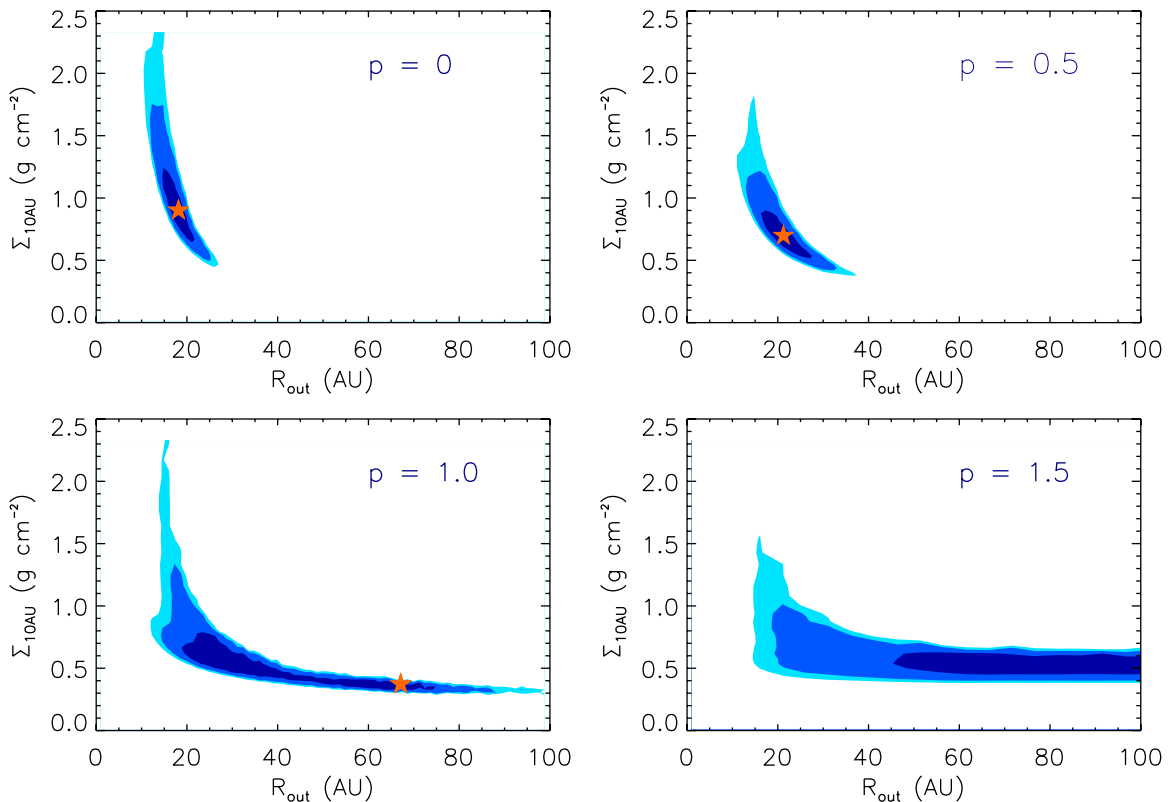
Figure 2. Contour plots of the χ^2-function projected into the $(R_{out}, \Sigma_{10\,AU})$ plane, for different p-values. The contours were drawn at $\Delta\chi^2$-values so that their projection on each axis gives the one-dimensional confidence intervals. These are drawn at the 68%, 90%, 95% confidence levels, going from the darkest to the lightest blue color, respectively. The best-fit models are represented by an orange star.

(A color version of this figure is available in the online journal.)

Table 1
Confidence Intervals for the Disk Outer Radii R_{out}
as Constrained by Our Analysis

| Confidence Level	R_{out} (AU)			
	$p = 0$	$p = 0.5$	$p = 1.0$	$p = 1.5$
68%	15–22	17–27	18–74	>45
90%	12–25	13–33	15–88	>18
95%	10–27	11–37	12–98	>15

values of $p = 0, 0.5, 1, 1.5$, similar to what found for disks around PMS stars (Guilloteau et al. 2011). We then launched several MCMC chains to check the convergence toward the absolute minimum of the χ^2-function in the $(\Sigma_{10\,AU}, R_{out}, i,$ P.A.) parameter space of the disk models. This method allows to efficiently probe the region of parameter space around the χ^2-absolute minimum, and to derive the confidence intervals for the fitting parameters (Isella et al. 2009).

Figure 2 shows the two-dimensional contour plots of the χ^2-function on the $(\Sigma_{10\,AU}, R_{out})$ parameter space for the different values of p. For a given p, there is a degeneracy between $\Sigma_{10\,AU}$ and R_{out}: for larger disks the disk surface density at a given radius has to decrease to conserve the total flux density which is proportional to the disk mass. There is also a clear correlation between p and the disk outer radius of the best-fit models: for disks with steeper radial surface densities, i.e., greater values of p, the disk has to be larger to conserve the total flux density, which is dominated by the outermost disk regions. Our observations do not have enough signal-to-noise ratio in

the faint outer regions of the disk, and the different p-values could not be discriminated by our data. This also means that the confidence intervals on R_{out} will depend on the adopted value of p. These intervals are listed in Table 1. In the case of $p = 0$ or 0.5, the disk outer radius is between about 15 and 27 AU (at 1σ). For larger values of p, larger disks are consistent with the data, and in the case of $p = 1.5$ only lower limits for R_{out} could be derived. The key point we want to highlight here is that for all the reasonable values of p we obtained a robust lower limit for $R_{out} > 10$ AU.

3.1. Grain Growth in the Outer Disk

Multi-wavelength observations of young disks in the sub-mm have been used to probe mm-sized grains in the disk (Beckwith & Sargent 1991). In the case of optically thin emission in the Rayleigh–Jeans part of the spectrum, the flux density of the disk is given by $F_\nu \propto \nu^{2+\beta}$ where β is the power-law index of the dust opacity $\kappa_\nu \propto \nu^\beta$. Deviations from the Rayleigh–Jeans regime can be accounted for by radiative transfer modeling of the dust emission, while the contribution from optically thick emission can be quantified via resolved images of the disk (Testi et al. 2003). Whereas tiny submicrometer-sized grains are characterized by relatively steep sub-mm spectral energy distributions with $\beta \approx 1.5$–2, shallower spectra with $\beta \approx 0$–1 have been typically found for young disks around PMS stars (Andrews & Williams 2005; Rodmann et al. 2006; Lommen et al. 2007; Ricci et al. 2010a, 2010b). This result has been generally interpreted as evidence for mm-sized grains, or larger,
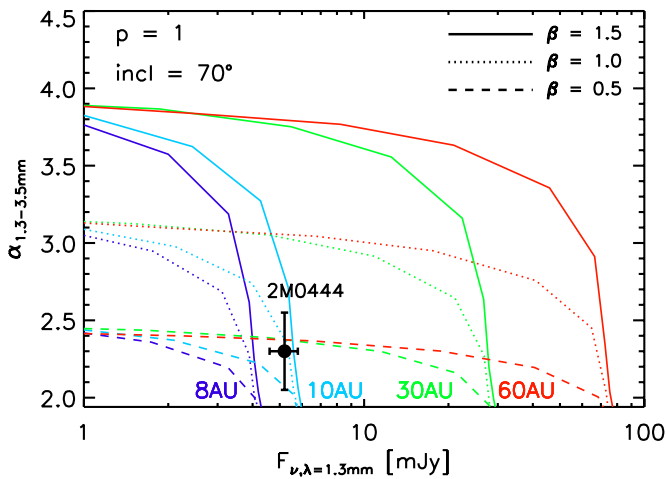
Figure 3. Submillimeter flux density vs. spectral index for disk models for 2M0444. The black dot shows the sub-mm data for 2M0444. Each line represents the prediction of disk models with the same disk outer radius and dust opacity spectral index β, as indicated on the plot, but increasing disk mass from left to right. Each model was computed by assuming a radial profile of the surface density $\Sigma \propto r^{-p}$, with $p = 1$, and a disk inclination of 70 deg. The adopted substellar properties and dust opacities are discussed in Section 3.

(A color version of this figure is available in the online journal.)

in the outer regions of the disk (Draine 2006; Natta et al. 2007; Ricci et al. 2012b).

While grain growth to mm-sized particles have been found for several dozens of disks around PMS stars, the very faint sub-mm fluxes of BD disks make their characterization much more challenging. If compared to typical T Tauri disks, BD disks allow to probe the coagulation of solids to lower gas and dust densities which are the most critical environments for the growth to mm-sized particles (Birnstiel et al. 2010). Also, models of dust dynamics predict that mm-sized particles should experience a faster inward radial drift in BD disks than in T Tauri disks (P. Pinilla et al., in preparation). Therefore, BD disks are ideal test beds for models of dust evolution in protoplanetary disks.

So far, conclusive evidence for the presence of mm-sized grains in a BD disk has been obtained only for ρ Oph 102 (Ricci et al. 2012a). They measured a sub-mm spectral index of 2.29 ± 0.16, and ruled out small (< 10 AU) optically thick disks from the analysis of the molecular CO emission. In the case of 2M0444, we measure a sub-mm spectral index of 2.30 ± 0.25 by combining our flux density measurement at 1.3 mm with 3.5 mm data obtained by Bouy et al. (2008), i.e., 0.55 ± 0.12 mJy. Figure 3 shows the measured flux density and sub-mm spectral index overlaid with the predicted sub-mm fluxes for models of disks around a BD with the same properties as 2M0444. The sub-mm photometry of 2M0444 can be explained by two classes of models: relatively small optically thick disks with an outer disk radius $R_{out} \approx 10$ AU, and larger, mostly optically thin disks with $R_{out} > 10$ AU. In the former case, the disk emission is insensitive to both disk mass and dust opacity κ_ν, and in fact all the possible values of β are consistent with the data. This shows how photometry alone is not sufficient to constrain grain sizes in disks (Testi et al. 2001).

At the same time our CARMA observations spatially resolved the dust emission and ruled out models with $R_{out} \lesssim 10$ AU: only the larger, mostly optically thin disk models with $\beta = 0.50 \pm 0.25$ are consistent with both photometric and interferometric data for the 2M0444 BD disk. This interval for β is consistent with most of the values constrained for protoplanetary disks

around PMS stars, and provides evidence for the presence of particles with sizes $\gtrsim 1$ mm in the outer regions of the 2M0444 BD disk.

Note that Figure 3 refers to disk models with a specific choice of the power law index of the dust surface density and disk inclination, i.e., $p = 1$ and $i = 70$ deg, respectively. However, these parameters are not observationally constrained. We found that the results presented above are not affected by our ignorance on these parameters by investigating their effect in the ranges of $p \in [0, 1.5]$, $i \in [0, 70]$ deg.[3]

3.2. Disk Mass and Outer Radius: Constraints on the Mechanisms of BD Formation

The analysis outlined above shows that the dust emission of the 2M0444 disk is mostly optically thin. This means that a dust mass can be estimated from the sub-mm fluxes. The β-values constrained by our analysis, i.e., $\beta = 0.50 \pm 0.25$, correspond to dust opacities values of $\kappa_{\nu,\lambda=1.3mm} \approx 0.2$–7 cm^2/g$_{dust}$ (Ricci et al. 2010b). We derive estimates for the dust mass of $\sim$1–30 M_{Earth}, or $\sim$0.3–10 M_{Jup} in gas assuming an ISM-like gas-to-dust mass ratio of 100. These values correspond to a disk with a mass of $\sim$0.6–20% of the mass of the BD, and are consistent with the distribution of values for more massive disks around PMS stars (Williams & Cieza 2011).

The constrained values for the disk radius, i.e., $R_{out} \approx 15$–30 AU for $p = 0, 0.5$ or $R_{out} > 20$ AU for $p = 1, 1.5$, are in line with previous estimates for BD disks detected with high-angular resolution optical imaging (Luhman et al. 2007a), CO molecular line (Ricci et al. 2012a), sub-mm photometry (Scholz et al. 2006). These values are very large for models of BD formation involving the ejection of pre-stellar objects in multiple systems, in which dynamical interaction during star–disk and disk–disk encounters significantly modifies the appearance of BD disks (e.g., Reipurth & Clarke 2001; Bate et al. 2003). For example, the numerical simulations by Bate et al. (2003) show that young BDs formed in this way are typically surrounded by relatively small disks with radii $\approx$10 AU, whereas only 5%–10% of their BD disks should have $R_{out} > 20$ AU. These numbers take in consideration the possible effect of viscous spreading which can lead to an increase of the disk size on a timescale comparable with the disk age. Furthermore, as noted in Bate et al. (2003), disks that were severely truncated and underwent following viscous spreading are expected to have a very low mass, because of both truncation and gas accretion during viscous evolution. This is not the case of 2M0444, whose disk-to-central object mass ratio inferred above is similar to what found for disks around PMS stars.

Here we note that the sample of BD disks for which some information on the disk radius has been obtained so far is strongly biased toward the sub-mm bright objects. These might also correspond to the population of relatively large disks predicted by models of BD formation involving ejection processes, whereas the smaller disks with radii $\lesssim$10 AU would likely be fainter and therefore not detected at sub-mm wavelengths. A high sensitivity and angular resolution survey of homogeneously selected BD disks in the sub-mm, e.g., with ALMA, is needed to constrain the predictions from these models on a statistical basis (Umbreit et al. 2011) and shed more light on the dominant channel for BD formation.

---

[3] The upper limit on the disk inclination comes from the low value of visual extinction of 2M0444, i.e., $A_V \approx 0$ (Luhman 2004): a more inclined disk would absorb a fraction of the substellar radiation and would not be consistent with optical spectroscopy (see Skemer et al. 2011).

4. SUMMARY

We present high angular resolution observations of the young BD disk 2M0444 obtained with CARMA at 1.3 mm. Our observations spatially resolve dust thermal emission for the first time for a disk around a BD. By analyzing the interferometric visibilities we infer disk radii of at least a few tens of AU for the 2M0444 disk. We find evidence for mm-sized grains, or larger, in the disk. Given the physical conditions in BD disks, i.e., lower densities and shorter timescales of solids drift than in typical T Tauri disks, this result provides the tightest test to models of dust evolution in disks, this topic being investigated in detail by Pinilla et al., in preparation.

REFERENCES

Andrews, S. M., & Williams, J. P. 2005, ApJ, 631, 1134
Apai, D., Luhman, K., & Liu, M. C. 2008, in ASP Conf. Ser. 384, 14th Cambridge Workshop on Cool Stars, Stellar Systems, and the Sun, ed. G. van Belle (San Francisco, CA: ASP), 383
Baraffe, I., Chabrier, G., Barman, T. S., Allard, F., & Hauschildt, P. H. 2003, A&A, 402, 701
Bate, M. R., Bonnell, I. A., & Bromm, V. 2003, MNRAS, 339, 577
Beckwith, S. V. W., & Sargent, A. I. 1991, ApJ, 381, 250
Birnstiel, T., Ricci, L., Trotta, F., et al. 2010, A&A, 516L, 14
Bouy, H., Huélamo, N., Pinte, C., et al. 2008, A&A, 486, 877
Chiang, E., & Goldreich, P. 1997, ApJ, 490, 368
Draine, B. T. 2006, ApJ, 636, 1114
Dullemond, C. P., Dominik, C., & Natta, A. 2001, ApJ, 560, 957
Guieu, S., Pinte, C., Monin, J.-L., et al. 2007, A&A, 465, 855
Guilloteau, S., Dutrey, A., Pitu, V., & Boehler, Y. 2011, A&A, 529, 105
Harvey, P. M., Henning, Th., Liu, Y., Ménard, F., et al. 2012, ApJ, 755, 67
Isella, A., Carpenter, J. M., & Sargent, A. I. 2009, ApJ, 701, 260
Klein, R., Apai, D., Pascucci, I., Henning, Th., & Waters, L. B. F. M. 2003, ApJ, 593, 57
Knapp, G. R., Leggett, S. K., Fan, X., et al. 2004, AJ, 127, 3553
Lommen, D., Wright, C. M., Maddison, S. T., et al. 2007, A&A, 462, 211
Luhman, K. L. 2004, ApJ, 617, 1216
Luhman, K. L. 2012, ARA&A, 50, 65
Luhman, K. L., Adame, L., D'Alessio, P., et al. 2007a, ApJ, 666, 1219
Luhman, K. L., Joergens, V., Lada, C., et al. 2007b, in Protostars and Planets V, ed. B. Reipurth, D. Jewitt, & K. Keil (Tucson, AZ: Univ. Arizona Press), 443
Natta, A., Testi, L., Calvet, N., et al. 2007, in Protostars and Planets V, ed. B. Reipurth, D. Jewitt, & K. Keil (Tucson, AZ: Univ. Arizona Press), 767
Pollack, J. B., Hollenbach, D., Beckwith, S., et al. 1994, ApJ, 421, 615
Reipurth, B., & Clarke, C. 2001, AJ, 122, 432
Ricci, L., Testi, L., Natta, A., & Brooks, K. J. 2010a, A&A, 521, 66
Ricci, L., Testi, L., Natta, A., Scholz, A., & de Gregorio-Monsalvo, I. 2012a, ApJL, 761, L20
Ricci, L., Testi, L., Natta, A., et al. 2010b, A&A, 512, 15
Ricci, L., Trotta, F., Testi, L., et al. 2012b, A&A, 540, 6
Rodmann, J., Henning, Th., Chandler, C. J., Mundy, L. G., & Wilner, D. J. 2006, A&A, 446, 211
Roeser, S., Demleitner, M., & Schilbach, E. 2010, AJ, 139, 2440
Scholz, A., Jayawardhana, R., & Wood, K. 2006, ApJ, 645, 1498
Skemer, A. J., Close, L. M., Szucs, L., et al. 2011, ApJ, 732, 107
Testi, L., Natta, A., Shepherd, D. S., & Wilner, D. J. 2001, ApJ, 554, 1087
Testi, L., Natta, A., Shepherd, D. S., & Wilner, D. J. 2003, A&A, 403, 323
Umbreit, S., Spurzem, R., Henning, Th., Klahr, H., & Mikkola, S. 2011, ApJ, 743, 106
Warren, S. G. 1984, ApOpt, 23, 1206
Weingartner, J. C., & Draine, B. T. 2001, ApJ, 548, 296
Williams, J. P., & Cieza, L. A. 2011, ARA&A, 49, 67
Zubko, V. G., Mennella, V., Colangeli, L., & Bussoletti, E. 1996, MNRAS, 282, 1321